

On the streaming motions of haloes and galaxies

Ravi K. Sheth¹, Antonaldo Diaferio², Lam Hui^{3,4} & Román Scoccimarro⁴

¹ *NASA/Fermilab Astrophysics Group, MS 209, Batavia, IL 60510-0500*

² *Dipartimento di Fisica Generale “Amedeo Avogadro”, Università di Torino, Italy*

³ *Department of Physics, Columbia University, 538 West 120th Street, New York, NY 10027*

⁴ *Institute for Advanced Study, School of Natural Sciences, Einstein Drive, Princeton, NJ 08540*

Email: sheth@fnal.gov, diaferio@ph.unito.it, scoccima@ias.edu, lhui@ias.edu

2000 October 5

ABSTRACT

A simple model of how objects of different masses stream towards each other as they cluster gravitationally is described. The model shows how the mean streaming velocity of dark matter particles is related to the motions of the parent dark matter haloes. It also provides a reasonably accurate description of how the pairwise velocity dispersion of dark matter particles differs from that of the parent haloes. The analysis is then extended to describe the streaming motions of galaxies. This shows explicitly that the streaming motions measured in a given galaxy sample depend on how the sample was selected, and shows how to account for this dependence on sample selection. In addition, we show that the pairwise dispersion should also depend on sample type. Our model predicts that, on small scales, redshift space distortions should affect red galaxies more strongly than blue.

Key words: galaxies: clustering – cosmology: theory – dark matter.

1 INTRODUCTION

Gravity makes objects cluster. Therefore, the motions of objects towards each other may provide information about the background cosmology. Of course, different subsets of the clustering particles may trace the underlying streaming motions differently. The scale dependence of the mean streaming $v_{12}^{\text{dm}}(r)$ of dark matter particles has been understood for some time now (Hamilton et al. 1991; Nityananda & Padmanabhan 1994). But there has been little study of how this statistic depends on trace-particle type.

To do this, we build a model in which gravitational clustering is viewed as the combination of two processes. The first arises from the fact that gravity causes matter to stream towards local minima of the gravitational potential. This requires a model of how matter which was initially distributed rather smoothly around the centre of collapse becomes redistributed into a more centrally concentrated density profile as the collapse proceeds. The second process is that these centres around which local collapses are occurring, these clusters, are themselves moving towards each other: clusters cluster. It is the combination of these two types of motions which gives rise to the spatial distribution and streaming motions of objects today.

Section 2.1 summarizes useful results which follow from linear theory. Section 2.2 shows how the streaming motions of collapsed dark matter haloes depend on halo mass. Section 2.3 uses this to model the streaming motions of parti-

cles, rather than haloes. It shows what fraction of a particle’s streaming motion arises from the motion of its parent halo, and what fraction must arise from motions within the halo. These smaller scale motions are essentially a consequence of the collapse around the halo centre we referred to earlier. It then presents measurements from numerical simulations which show that the model predictions are reasonably accurate. It also shows that the model provides a reasonable description of how the second moment of the pairwise velocity distribution of the dark matter differs from that of haloes.

Section 3 shows how to extend the model to study the mean streaming motions and the pairwise velocity dispersion of galaxies and presents measurements from semianalytic galaxy formation simulations which show that the model predictions are reasonably accurate. Section 4 discusses what this model implies if one wishes to use measurements of the streaming motions of galaxies to make inferences about cosmology.

2 THE MODEL

2.1 The mean streaming velocity

We will begin by reviewing the strategy which led to the derivation of how $v_{12}^{\text{dm}}(r)$ depends on scale. The relevant starting equation is the pair conservation equation in Peebles’ book (Peebles 1980), but we will start with the equa-

arXiv:astro-ph/0010137v2 8 Oct 2000

tion in the form presented by Nityananda & Padmanabhan (1994):

$$\frac{\partial (1 + \bar{\xi})}{\partial \ln a} = -\frac{v_{12}(r)}{Hr} 3 \left[1 + \xi(r) \right] \quad (1)$$

where $\bar{\xi}(r, a)$ is the volume averaged correlation function on proper (rather than comoving) scale r at the time when the expansion factor is a , and the Hubble constant is H . This says that if we know the correlation function for all scales r and all times a , then the assumption that the number of pairs is conserved allows us to compute how $v_{12}(r)$ depends on scale today.

An approximate solution to this expression can be got as follows (Peebles 1980). Assume that $\bar{\xi}$ evolves according to linear theory: $\bar{\xi}(r, a) = [D(a)/D_0]^2 \bar{\xi}(r, a_0)$, where $D(a)$ is the linear theory growth factor at a , and D_0 is the growth factor at the present time when $a = a_0$. In an Einstein de-Sitter cosmology, $D(a)/D_0 = a/a_0$. Then the left hand side is $\partial \bar{\xi}(r, a)/\partial \ln a = 2 f(\Omega) \bar{\xi}(r, a)$, where $f(\Omega) \equiv \partial \ln D/\partial \ln a$. So, in this approximation we get

$$-\frac{v_{12}(r)}{Hr} = \frac{2f(\Omega)}{3} \frac{\bar{\xi}(r, a)}{1 + \xi(r, a)}. \quad (2)$$

On large scales, $\xi \ll 1$, and so this is just the usual linear theory expression with an extra factor of $(1 + \xi)$ in the denominator. While this approximation is fine on large scales ($r \geq 10$ Mpc/h), it underestimates the exact solution by a factor of 3/2 or so on smaller scales (Juszkiewicz, Springel & Durrer 1998; Sheth et al. 2000).

Hamilton et al. (1991) showed they could compute a good estimate of the evolution of $\xi(r, a)$, if the initial correlation function is known (also see Nityananda & Padmanabhan 1994). Hamilton et al. also showed that by inserting their expression for the evolution of $\xi(r, a)$ into equation (1) above, they were able to describe the shape of $v_{12}^{\text{dm}}(r)$ well on all scales.

While this approach is very useful for studying the statistics of dark matter particles, it is not obvious that it can be used to estimate the streaming motions of galaxies. This is because one usually assumes that galaxies form at different times. This means that the number of galaxies is not conserved, so the number of galaxy pairs is not conserved. This means, for example, that the correlation function of galaxies refers to different sets of particles at different times. Therefore, there is little reason to expect that inserting the correlation function of galaxies into the pair conservation equation should provide a good estimate of $v_{12}^{\text{gal}}(r)$ today. We show below that, provided one makes the correct choice of what one uses for $\xi_{\text{gal}}(r, a)$, the pair conservation equation can be used to provide an accurate estimate of the streaming motions of galaxies.

2.2 The haloes

This subsection is concerned with the first moment of the pairwise velocity distribution of haloes identified at the present time. Every halo will be represented by one particle, say, the one at the halo centre of mass today. Imagine tracing these centre-of-mass particles back in time. By definition the number of these particles is conserved, since all we're doing is following them back to high redshift. Of course, at high redshift, few if any of the haloes would actually have

collapsed around these centre-of-mass particles. Nevertheless, we will use the motions of these particles to represent the motions of the halo centre of mass. Peebles' pair conservation equation, combined with the assumption that the motion of a halo today is the same as that of its associated centre-of-mass particle, says that if we knew $\xi(r, a)$ for these tracer particles, then we can compute $v_{12}^{\text{halo}}(r)$ today.

So, to compute v_{12}^{halo} , we are stuck with the problem of studying the spatial distribution (i.e., the bias factor) of a special marked set of particles at earlier times. The case in which the marked particles (in this case, the halo centres-of-mass) are observed at a later epoch than when they were marked is familiar: e.g. this is like the Mo & White (1996) simple model for galaxies, in which galaxies formed in haloes at $z = 3$ but we only observe them today. Here, we are interested in the spatial distribution of the special particles at earlier epochs than when they were marked.

The halo centre-of-mass particles are biased tracers of the dark matter distribution. The large scale bias factor is the square root of the ratio of the correlation function of these particles to that of the dark matter correlation function on large scales. It depends on halo mass:

$$\xi_{\text{hh}}(r) \approx b^2(m) \xi_{\text{dm}}^{\text{Lin}}(r), \quad (3)$$

and a similar equality holds for $\bar{\xi}_{\text{hh}}(r)$. Here $\xi_{\text{dm}}^{\text{Lin}}(r)$ denotes the initial correlation function of the dark matter extrapolated using linear theory to the present time. In equation (3) we use the linearly extrapolated $\xi_{\text{dm}}^{\text{Lin}}(r)$ rather than the present day $\xi(r)$ as a practical way of taking into account the volume exclusion effects of haloes at small scales. See Section 2 in Sheth et al. (2000) for a detailed discussion.

To a good approximation,

$$b(m) = 1 + \frac{\nu^2(m) - 1}{\delta_{\text{c0}} D(a)/D_0}, \quad (4)$$

where $\nu(m) \equiv \delta_{\text{c0}}/\sigma(m)$ is a function which increases with decreasing halo mass, and $D(a)$ and D_0 were defined earlier. At the present time, $D(a) = D_0$ and this is the familiar Eulerian bias formula from Mo & White (1996). The Lagrangian bias factor is usually expressed as the ratio of ξ_{hh} at the initial time to the linearly extrapolated $\xi_{\text{dm}}^{\text{Lin}}$. This means that the Lagrangian bias factor is

$$b_{\text{Lag}}(m) = \sqrt{\frac{\xi_{\text{hh}}(r)}{\xi_{\text{dm}}^{\text{Lin}}(r)}} \frac{D(a_i)}{D_0} = \frac{D(a_i)}{D_0} + \frac{\nu^2(m) - 1}{\delta_{\text{c0}}}$$

where a_i denotes the expansion factor at the initial time. Since $a_i \ll a_0$, $b_{\text{Lag}} \rightarrow (\nu^2 - 1)/\delta_{\text{c0}}$, which is another familiar expression from Mo & White (1996). So, in this approximation,

$$\frac{\partial b(m)}{\partial \ln a} = f(\Omega) \left[1 - b(m) \right]. \quad (5)$$

It is straightforward to insert these expressions for the halo correlation function and its evolution into the pair conservation formula (equation 1) to see how different v_{12}^{halo} is from v_{12}^{dm} . If we study the streaming motions of haloes of two different masses, then we must replace $b^2(m) \rightarrow b(m_1)b(m_2)$. This gives

$$\frac{v_{12}^{\text{halo}}(r)}{Hr} = \frac{v_{12}^{\text{dm}}(r)}{Hr} \frac{b_1 b_2 [1 + \xi_{\text{dm}}^{\text{Lin}}(r)]}{[1 + b_1 b_2 \xi_{\text{dm}}^{\text{Lin}}(r)]}$$

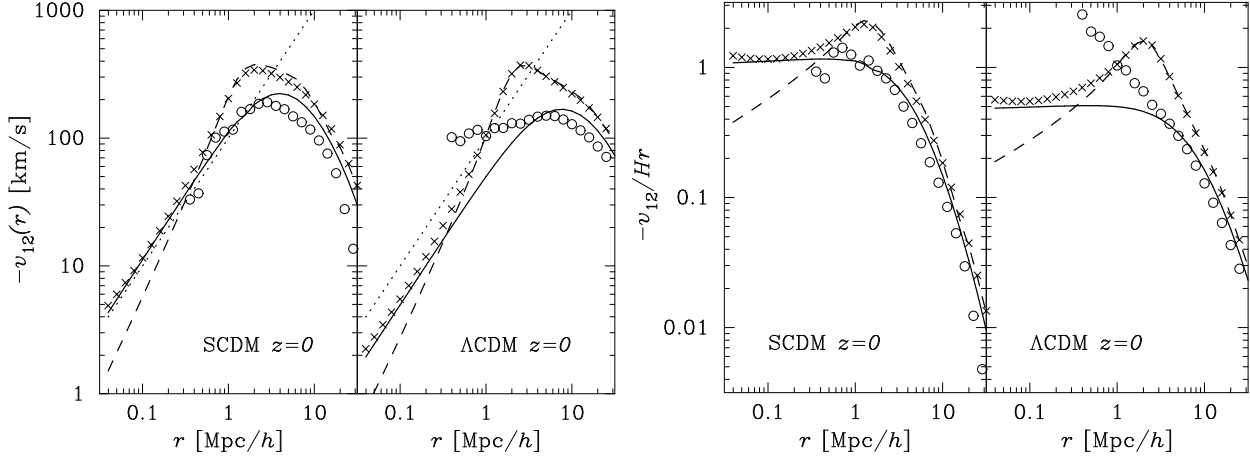


Figure 1. Mean streaming motions in the GIF simulations. Open circles and crosses show the streaming motions of the haloes and the dark matter, respectively. Solid and dashed curves show our predictions for the haloes (equation 8), which should be accurate on large scales, and the dark matter (the sum of equations 9 and 10), which should be accurate on all scales. Dotted lines show the Hubble velocity for comparison.

$$-\frac{f(\Omega)\bar{\xi}_{\text{dm}}^{\text{Lin}}(r)[b_1(1-b_2)+b_2(1-b_1)]}{3[1+b_1b_2\xi_{\text{dm}}^{\text{Lin}}(r)]}. \quad (6)$$

If we insert the linear evolution approximation for the relation between the correlation function and v_{12} (equation 2), then this becomes

$$\frac{v_{12}^{\text{halo}}(r)}{Hr} \approx \frac{v_{12}^{\text{dm}}(r)}{Hr} \left(\frac{b_1+b_2}{2} \right) \frac{1+\xi_{\text{dm}}^{\text{Lin}}(r)}{1+b_1b_2\xi_{\text{dm}}^{\text{Lin}}(r)}. \quad (7)$$

Notice that when $b_1 = b_2 = 1$, then $v_{12}^{\text{halo}}(r) = v_{12}^{\text{dm}}(r)$. Also, in the large separation (small ξ) limit, $v_{12}^{\text{halo}}(r) \rightarrow (b_1+b_2)/2$ times $v_{12}^{\text{dm}}(r)$. So, on average and on large separations, relative to the dark matter, massive haloes $(b_1+b_2) > 2$ stream towards each other whereas less massive haloes $(b_1+b_2) < 2$ stream away from each other. This makes some physical sense; clusters cluster, so they are moving towards each other, whereas smaller clumps are in or at the edges of expanding voids, so they are separating from each other. This linear bias of the streaming velocities at large separation is consistent with the linear theory analysis of Fisher et al. (1994).

Notice that v_{12} scales with the sum of the bias factors. If one ignored the evolution of the bias factor when using equation (2), one would have concluded that the scaling was with the product of the bias factors—including the evolution of the bias factor is essential to getting the correct answer. Finally, notice that on smaller scales where $\xi_{\text{dm}}^{\text{Lin}} > 1$, this analysis suggests that v_{12} of less massive haloes should be larger than that of the dark matter, with the opposite trend being true for massive haloes. Of course, the linear theory and linear evolution approximations we used to obtain equation (7) are not accurate on small scales. Nevertheless, this provides at least some indication of the small scale behaviour of the halo streaming motions.

Fig. 1 compares this model with measurements in the SCDM and Λ CDM GIF (Kauffmann et al. 1999) simulations which were run by the Virgo collaboration (Jenkins et al. 1999) and are now available to the public. The open circles show the streaming motions of all the haloes with $m > 2 \times 10^{11} M_{\odot}/h$ and $m > 8.4 \times 10^{11} M_{\odot}/h$ in the SCDM and the Λ CDM simulations, and the solid line shows what our model

predicts. Specifically, it shows

$$\begin{aligned} -\frac{V_{12}^{\text{halo}}(r)}{Hr} &\equiv -\int dm_1 \int dm_2 \frac{v_{12}^{\text{halo}}(r)}{Hr} \\ &\times \frac{n(m_1)n(m_2)[1+b(m_1)b(m_2)\xi_{\text{dm}}^{\text{Lin}}(r)]}{\bar{n}_{\text{halo}}^2[1+b_{\text{halo}}^2\xi_{\text{dm}}^{\text{Lin}}(r)]} \\ &= \frac{2f(\Omega)}{3} \frac{b_{\text{halo}}\bar{\xi}_{\text{dm}}^{\text{Lin}}(r)}{1+b_{\text{halo}}^2\xi_{\text{dm}}^{\text{Lin}}(r)}. \end{aligned} \quad (8)$$

where $\bar{n}_{\text{halo}} \equiv \int dm n(m)$ is the average number density of haloes, $b_{\text{halo}} \equiv \int dm n(m)b(m)$ is their average bias factor, the weighting factor in the second line is the ratio of the number of m_1 and m_2 halo pairs at r to the total number of halo pairs at r , and the final expression follows from inserting equation (7) for v_{12}^{halo} and using equation (2) for v_{12}^{dm} . Our model, which we only expect to be accurate on large scales because our approximation for the halo correlation function, equation (3), breaks down on small scales, is reasonably accurate down to scales of order a Mpc/h or so. For comparison, the dotted curves show the Hubble velocity. The crosses show the streaming motions of the dark matter particles in the simulations, and the dashed curve shows the prediction associated with the model described in the next section.

2.3 The dark matter

The large scale net streaming motion of the dark matter can be got from our expression for the halo motions by integrating up the contribution to the streaming motion from pairs in different mass haloes, weighting by the fraction of the total number of pairs which are in such haloes, and weighting by the halo mass function:

$$\begin{aligned} -\frac{v_{12}^{\text{halo}}(r)}{Hr} &= -\int dm_2 \int dm_1 \frac{m_1 n(m_1)}{\bar{\rho}} \frac{m_2 n(m_2)}{\bar{\rho}} \\ &\times \frac{[1+b(m_1)b(m_2)\xi_{\text{dm}}^{\text{Lin}}(r)]}{1+\xi_{\text{dm}}(r)} \frac{v_{12}^{\text{halo}}(r)}{Hr} \\ &= -\frac{v_{12}^{\text{dm}}(r)}{Hr} \frac{1+\xi_{\text{dm}}^{\text{Lin}}(r)}{1+\xi_{\text{dm}}(r)}. \end{aligned} \quad (9)$$

The final equality follows from inserting equation (6), noting that $\int dm mn(m) \equiv \bar{\rho}$, and using the fact that the bias factors are defined so that $\int dm mn(m) b(m) \equiv \bar{\rho}$.

We can now make two important points. The first is that, at large separations, this expression equals $v_{12}^{\text{dm}}(r) = v_{12}^{\text{2halo}}(r)$; in this regime the streaming motions of the dark matter particles are entirely due to the fact that the haloes which contain the particles are moving. Moreover, in this regime, $v_{12}^{\text{dm}}(r) \approx v_{12}^{\text{L}}(r)$, where v_{12}^{L} is got from equation (2) by using the linear theory values of ξ and $\bar{\xi}$. The second is that this expression exactly equals that in Sheth et al. (2000) for the contribution to $v_{12}(r)$ from particles which are in separate haloes (see their eq. 19). This will be important in what follows.

Notice that on smaller scales, $\xi_{\text{dm}}^{\text{Lin}}(r) < \xi_{\text{dm}}(r)$. In this regime the halo motions only account for a fraction of $v_{12}^{\text{dm}}(r)$. The remaining contribution to $v_{12}^{\text{dm}}(r)$ must arise from the streaming motions of pairs in which both particles are in the same halo. This means that the fact that our model for halo motions is not accurate on small scales will not matter very much for the small scale value of v_{12}^{dm} because, on small scales, the fraction of pairs which are in separate haloes, and so are affected by this inaccuracy, is small. We turn, therefore, to a discussion of the streaming motions of pairs in which both particles are in the same halo.

If haloes are stable, then the streaming motion within a halo exactly cancels the Hubble flow: $-v_{12}(r)/Hr = 1$. In this case, the contribution from pairs which are in the stable haloes equals unity times

$$\int dm \frac{m^2 n(m)}{\bar{\rho}^2} \frac{\lambda(r|m)}{1 + \xi_{\text{dm}}(r)} = \frac{\xi_{1\text{halo}}(r)}{1 + \xi_{\text{dm}}(r)},$$

where $m^2 \lambda(r|m)$ denotes the number of pairs at separation λ which are in the same halo which has mass m ; it depends on the density profiles of haloes. For all halo shapes of interest, this expression approaches unity at very small r , because $\xi_{\text{dm}}(r) = \xi_{1\text{halo}}(r) + \xi_{\text{dm}}^{\text{Lin}}(r) \approx \xi_{1\text{halo}}(r)$, and $\xi_{\text{dm}}(r) \gg 1$ on scales which are smaller than a typical halo. So, if stable clustering is correct, then $-v_{12}^{\text{dm}}(r)/Hr = 1$ on small scales. In fact, the mean pairwise velocity on small scales depends on the low-mass behaviour of $n(m)$ and $\lambda(r|m)$ —in general, there is no guarantee that $n(m)$ and $\lambda(r|m)$ will conspire to give stable clustering (Ma & Fry 2000; Sheth et al. 2000).

In particular, Section 4 of Sheth et al. (2000) shows that the small scale term is

$$\begin{aligned} -\frac{v_{12}^{\text{1halo}}}{Hr} &= \frac{\partial}{\partial \ln a} \int dm \frac{m^2 n(m, a)}{\bar{\rho}^2} \int_0^r \frac{dy}{r} \frac{y^2}{r^2} \frac{\lambda(y|m, a)}{[1 + \xi(r, a)]} \\ &= \frac{\partial \ln m_*(a)}{\partial \ln a} \frac{[\bar{\xi}_{1\text{halo}}(r, a) - \xi_{1\text{halo}}(r, a)]}{3[1 + \xi(r, a)]}, \end{aligned} \quad (10)$$

where $\lambda(r|m, a)$ is proportional to the number of pairs in the same m -halo which have separation r , and $n(m, a)$ is the number density of virialized m -haloes at time a . (Our notation differs slightly from that in Sheth et al.—they absorbed the two factors of m into their definition of λ , whereas here we have chosen to show these factors explicitly. Hence, our $m^2 \lambda$ is their λ .) In Sheth et al., $n(m, a)$ depended on time, and the halo profile did as well, because virialized haloes were assumed to have profiles of the form given by Navarro, Frenk & White (1997), and these halo shapes depend both on $m/m_*(a)$ and on the ratio of the average density within

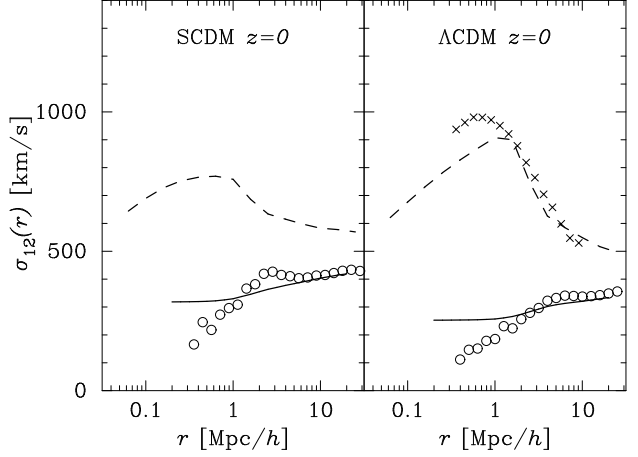


Figure 2. Pairwise dispersions in the GIF simulations. Open circles and crosses show the streaming motions of the haloes and the dark matter, respectively. Solid and dashed curves show predictions for the haloes and the dark matter (from Sheth et al. 2000).

the virialized halo to the background density at the time it virialized. (Strictly speaking, the expression above assumes that all of the time dependence of the halo shape can be written as a function of m/m_* —see Sheth et al. for details.)

The sum of equations (9) and (10) gives a complete description of the streaming motions of dark matter on all scales. The dashed curves in Fig. 1 show that this sum provides a good description of the dark matter streaming motions on all but the smallest scales (see Sheth et al. 2000 for a discussion of the discrepancy at the smallest scales). Now, the dashed curves correspond to independently identifying haloes at each epoch. On the other hand, we could have followed the approach of Section 2.2—identify or mark the haloes today, and then follow them backward in time. With this latter approach, the number density of haloes is fixed to the value today, $n(m, a_0)$, but the profile changes from, say a tophat to a more centrally concentrated shape. Equation (9) shows that the contribution to the streaming motions from particles in separate haloes is independent of the details of how this happens. However, recall that this contribution exactly equals the two-halo contribution to v_{12}^{dm} worked out by Sheth et al. (2000). This means that the one-halo contributions to v_{12} must also be the same in both approaches. In particular, this means that however the profile changes from a tophat to an NFW shape, it must change in just such a way that the final answer for the streaming motions of the dark matter particles equals equation (10). Indeed, we can use this requirement to constrain how the profile changes from the initial tophat to the final NFW cusp—the Appendix shows a worked example of how to do this.

2.4 The pairwise velocity dispersion

So far, we have shown how the mean streaming motions of the dark matter and the haloes are related. Sheth et al. (2000) discuss how to do this for the second moment of the pairwise velocity distribution. They argued that the dark matter particles receive substantial nonlinear kicks to their initial velocities (essentially, the virial motions within

haloes), whereas the haloes do not (Sheth & Diaferio 2000). As a result the pairwise dispersion of the dark matter should be significantly larger than that of the haloes on all scales.

Fig. 2 compares what their equation (31) predicts with the simulations (we refer the reader to their paper for details of the model). The open circles and crosses show the pairwise dispersion, $\sigma_{12}(r)$, of the haloes and the dark matter respectively, and the dashed and solid curves show the model predictions. (We do not show σ_{12} for the dark matter in the SCDM simulations because the simulation box is sufficiently small [85Mpc/h] that cosmic variance affects the measurement significantly.) The model is reasonably accurate on large scales, and not accurate on small scales. Sheth et al. (2000) discuss why this happens for the dark matter (the inaccuracy is due to the simplifying assumptions that haloes have no substructure, the pairwise dispersion from a single halo is isotropic and independent of the pair position, and the number of pairs in the infall regime around haloes is sufficiently small that the use of virial motions to model the dispersion from infalling pairs does not lead to a large error). For the haloes, this discrepancy appears on scales which are of the order of a typical m_* halo and smaller. This suggests that the discrepancy almost surely arises from using linear theory to model the spatial distribution and velocities of haloes on scales which are smaller than the smoothing scale used to make the model prediction. Despite the quantitative discrepancies on small scales, the model is in qualitative agreement with the simulation: the pairwise dispersion of the haloes is substantially smaller than that of the dark matter.

3 GALAXIES

The previous section showed that the first moment of the pairwise velocity distribution of haloes is different from that of the dark matter. It showed that massive haloes separated by large distances are streaming together more rapidly than less massive haloes at the same separation, and that this difference scaled with one rather than two powers of the halo bias factor. It also showed that the dark matter statistic was obtained by weighting the halo statistic by the number of dark matter particle pairs per halo. The second moments of the pairwise velocity distributions are also different. In this case, also, the dark matter statistic is got by weighting by the number of particle pairs per halo. However, the pairwise dispersion is also sensitive to the fact that virial motions within haloes can be substantially higher than the motions of the haloes themselves. As a result, the pairwise velocity dispersion of dark matter particles is substantially larger than that of haloes, on all scales. This section studies what these results imply for the pairwise motions of galaxies.

We will model galaxies as random particles in dark matter haloes. That is, the motion of the galaxies is the same as that of the dark matter particle with which they are associated. In this sense there is no velocity bias in our model; the fact that velocity statistics for the dark matter and the galaxies may, nevertheless, be different, arises solely from the fact that dark matter statistics weight each halo proportional to halo mass, whereas galaxy statistics do not. Such models for the difference between the statistics of galaxies and dark matter particles have received considerable atten-

tion recently. Seljak (2000), Peacock & Smith (2000) and Scoccimarro et al. (2000) have used them to model the spatial distribution of galaxies, Sheth & Diaferio (2000) describe how to model the distribution function of galaxy peculiar velocities, and Sheth et al. (2000) describe how to use these models to do analytically what Jing, Mo & Börner (1998) did numerically in their study of the pairwise velocity dispersion of galaxies.

Within the context of this model, galaxies are treated by setting

$$v_{12}^{\text{gal}}(r) = v_{12}^{\text{1gal}}(r) + v_{12}^{\text{2gal}}(r), \quad (11)$$

where the two terms denote the contribution to the statistic from galaxies in the same and in different haloes, respectively. The second term on the right hand side can be got by modifying equation (9):

$$\begin{aligned} \frac{v_{12}^{\text{2gal}}(r)}{Hr} &= \int dm_2 \int dm_1 \frac{g(m_1)n(m_1)}{\bar{\rho}_{\text{gal}}} \frac{g(m_2)n(m_2)}{\bar{\rho}_{\text{gal}}} \\ &\times \frac{[1 + b(m_1)b(m_2)\xi_{\text{dm}}^{\text{Lin}}(r)]}{1 + \xi_{\text{gal}}(r)} \frac{v_{12}^{\text{halo}}(r)}{Hr} \end{aligned} \quad (12)$$

where

$$\begin{aligned} \bar{\rho}_{\text{gal}} &= \int dm g(m)n(m) \quad \text{and} \\ \xi_{\text{gal}}(r) &= \int dm \frac{g_2(m)n(m)}{\bar{\rho}_{\text{gal}}} \frac{\lambda(r|m)}{\bar{\rho}_{\text{gal}}} \\ &+ \int dm_2 \int dm_1 \frac{g(m_1)n(m_1)}{\bar{\rho}_{\text{gal}}} \frac{g(m_2)n(m_2)}{\bar{\rho}_{\text{gal}}} \\ &\times [b(m_1)b(m_2)\xi_{\text{dm}}^{\text{Lin}}(r)] \\ &\equiv \xi_{\text{gal}}^{\text{halo}}(r) + b_{\text{gal}}^2 \xi_{\text{dm}}^{\text{Lin}}(r). \end{aligned} \quad (13)$$

Here $g(m)$ and $g_2(m)$ denote the first and second moments of the distribution of the number of galaxies in m -haloes, and we set $g_2(m) = 0$ if $g(m) < 1$. There are details associated with how one treats the central galaxy in a halo, but, for the most part, these amount to a small effect (see Sheth & Diaferio 2000), so we have ignored them—they add complications but no essential change to the logic of our argument.

On scales larger than a few Mpc/h, v_{12}^{2gal} dominates over the one-halo contribution. If we assume linear theory for the evolution of the two-halo term (equation 2), then we can set $2f(\Omega)\xi_{\text{dm}}^{\text{Lin}}/3 \rightarrow -v_{12}^{\text{dm}}/Hr$ times $1 + \xi_{\text{dm}}^{\text{Lin}}(r)$, and then equation (12) reduces to

$$\frac{v_{12}^{\text{2gal}}(r)}{Hr} \approx \frac{v_{12}^{\text{dm}}(r)}{Hr} b_{\text{gal}} \left[\frac{1 + \xi_{\text{dm}}^{\text{Lin}}(r)}{1 + \xi_{\text{gal}}(r)} \right]. \quad (14)$$

This shows that, on large scales, the streaming motions of galaxies can be biased relative to the dark matter. The extent to which they are biased is related to how differently they are clustered, and this, in turn, depends on the $g(m)$ relation.

On smaller scales, the streaming motions are dominated by galaxy pairs in which both members are in the same halo. A little thought shows that this can be computed simply by setting $\bar{\rho} \rightarrow \bar{\rho}_{\text{gal}}$ and $m^2 \rightarrow g_2(m)$ in equation (10). This is because the $g(m)$ relation does not introduce any additional time dependence—recall that the number density of haloes in the present model is fixed to the value it has today, and

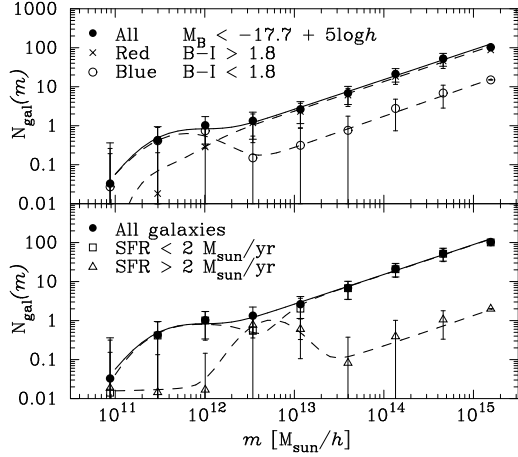


Figure 3. Mean number of bright galaxies as a function of parent halo mass in the Λ CDM GIF semianalytic galaxy formation model of Kauffmann et al. (1999). Top panel shows the result of dividing the sample into two based on colour. Bottom panel shows a division based on star formation rate. Crosses, circles, squares and triangles are for objects classified as being red, blue, quiescent and star-forming galaxies respectively.

the galaxies are to be thought of simply as marked tracer particles within the haloes.

This has an interesting consequence. Suppose one wishes to use the pair conservation equation (1) to estimate $v_{12}^{\text{gal}}(r)$. Then the model above suggests that, on small scales, simply inserting the observed galaxy correlation function into equation (1) should be reasonably accurate. However, on larger scales, doing this leads to an estimate of v_{12}^{gal} which is incorrect, for the following reason. Because there is no time dependence in $g(m)$, the result of doing this has the same time dependence as in the case of the dark matter for which $g(m) = m$, or the case of the haloes for which $g(m) = 1$. But we know that, for the haloes, doing this results in the wrong answer, because it neglects the evolution of the bias factor. The case of galaxies is no different; if we insert the observed galaxy correlation function into the pair conservation equation, then we are incorrectly neglecting the evolution of the bias factor of the galaxies. This would lead one to conclude, incorrectly, that v_{12} should scale as b_{gal}^2 rather than as b_{gal} .

3.1 Comparison with simulations

To illustrate how our model works, we will use the $g(m)$ relations we obtained from the semianalytic GIF Λ CDM model of Kauffmann et al. (1999) which are now publicly available. Sheth & Diaferio (2000) provide a fitting formula for the $g(m)$ relation of a GIF galaxy catalog which was constructed by choosing all galaxies brighter than $M_V = -17.7 + 5 \log h$, after accounting for the effects of dust. We divided that catalog up into two subsamples based on colour (galaxies labelled as being redder or bluer than $B - I = 1.8$) and on star-formation rate (rates greater or less than $2M_{\odot}/\text{yr}$). Fig. 3 shows these relations. The dashed lines show the following fits:

$$N_{\text{All}}(m) = (m_{11}/700)^{0.9} + 0.5 e^{-4[\log_{10}(m_{11}/5.6)]^2}$$

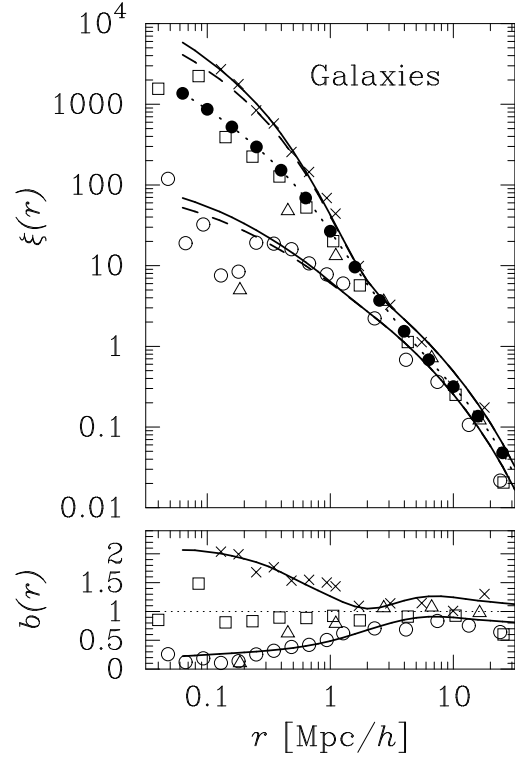


Figure 4. Correlation functions of different tracers of the dark matter density field in the Λ CDM GIF semianalytic galaxy formation model. Filled circles are for the dark matter, crosses are for red galaxies, squares for galaxies which have low star formation rates, triangles for galaxies with high star formation rates, and open circles for blue galaxies. The two solid curves show our model predictions for the red and blue galaxies, and the dashed curves show what happens if we use the second factorial moment of the galaxy counts, rather than the second moment when making our model prediction. For comparison, the dotted curve shows the predicted dark matter correlation function.

$$\begin{aligned}
 N_{\text{Blue}}(m) &= (m_{11}/500)^{0.8} + 0.6 e^{-4[\log_{10}(m_{11}/6.2)]^2} \\
 N_{\text{Red}}(m) &= N_{\text{All}}(m) - N_{\text{Blue}}(m) \\
 N_{\text{hSFR}}(m) &= 0.015 + (m_{11}/7000)^{0.9} + e^{-8[\log_{10}(m_{11}/56.2)]^2} \\
 N_{\text{ISFR}}(m) &= N_{\text{All}}(m) - N_{\text{hSFR}}(m)
 \end{aligned} \tag{15}$$

where m_{11} is the halo mass in units of $10^{11}M_{\odot}/h$. The solid lines are the same in both panels; they show $N_{\text{All}}(m)$, and they equal the sum of the two dashed lines. These relations can be used to compute the statistics of one of these galaxy samples, rather than dark matter particles, by setting $g(m)$ equal to the appropriate $N_{\text{gal}}(m)$ relation.

In addition to these mean $N_{\text{gal}}(m)$ relations, our models also require the second moment of the number of galaxies per halo distribution. We have approximated it by setting $g_2(m) = 0$ if $g(m) < 1$, and

$$g_2(m) = \mu^2(m) g^2(m) + \mu g(m) \quad \text{if } g(m) \geq 1, \tag{16}$$

where $\mu(m) = \log_{10}[20g(m)]^{1/2}$ if $g(m) \leq 5$, and $\mu = 1$ when $g(m)$ is larger. Because $\mu = 1$ for a Poisson distribution, this approximately accounts for the fact that the scatter in galaxy counts is sub-Poisson in low mass haloes. If we

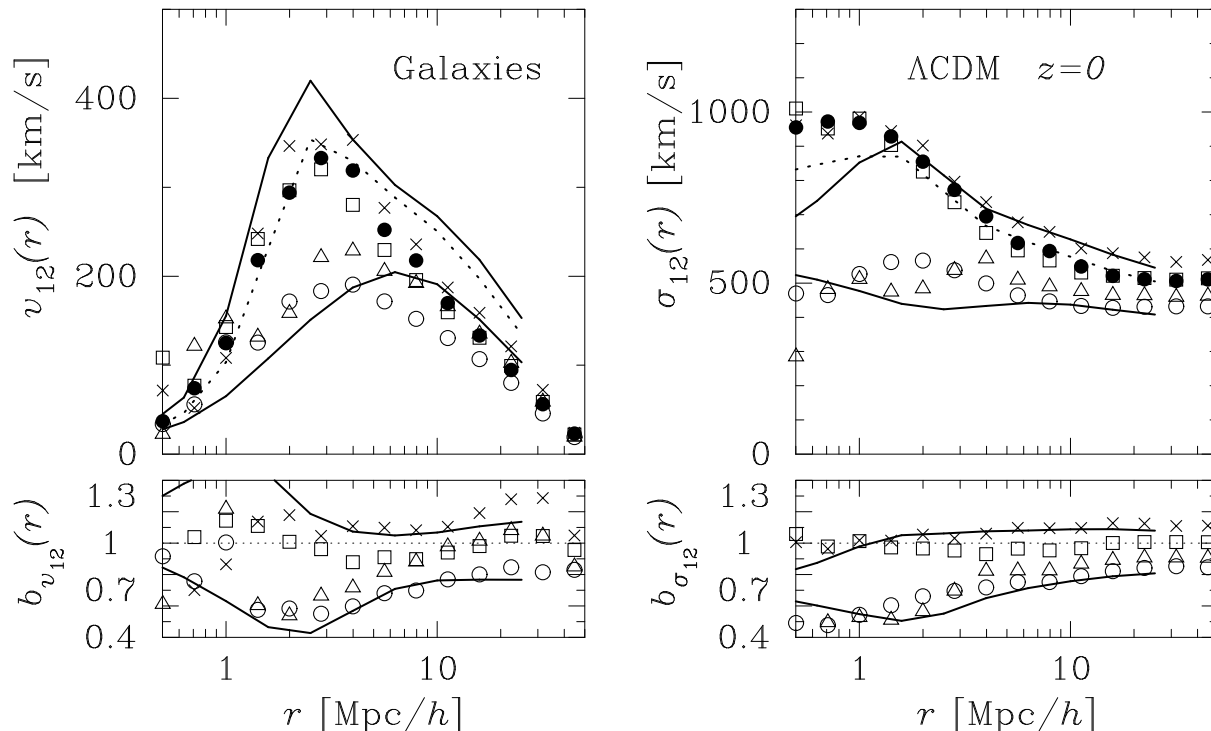


Figure 5. The mean streaming velocity (left) and pairwise velocity dispersion (right) in the Λ CDM GIF semianalytic galaxy formation model. Filled circles are for the dark matter, crosses are for red galaxies, squares for galaxies which have low star formation rates, triangles for galaxies with high star formation rates, and open circles for blue galaxies. The solid and dotted curves show our predictions for the red and blue galaxies, and the dark matter, respectively.

use the same galaxy sample that Scoccimarro et al. (2000) did, then our model for the scatter is similar to theirs.

The correlation functions for these four subsamples are shown in Fig. 4: crosses, open circles, triangles and squares show $\xi_{\text{gal}}(r)$ for red, blue, star-forming and quiescent galaxies in the GIF simulation. Filled circles show the correlation function of the dark matter particles. Notice how similar the correlation function of the blue sample is to that of the star-forming sample, how similar the red and quiescent samples are, and how different the blue and star-forming samples are from the red and quiescent samples.

The two solid curves show the result of using our model to compute the correlation functions of the red and blue samples, because these differ the most from each other. We did this by setting $g(m)$ in equation (13) equal to the appropriate $N_{\text{gal}}(m)$ relation. For comparison, the dashed curves show the result of using the second factorial moment, rather than the second moment, when computing the galaxy correlation functions; the difference only matters on small scales. The dotted curve shows our calculation of $\xi_{\text{dm}}(r)$ which has $g(m) = m$. The bottom panel shows how $b \equiv \sqrt{\xi_{\text{gal}}/\xi_{\text{dm}}}$ (the ratio of the solid and dotted curves) depends on scale. Both panels show that our model provides a good description of the simulation results. In computing our model predictions, we assumed that the two samples both trace their parent dark matter haloes similarly. That is, we used the same function $\lambda(r|m)$ for both the red and the blue samples. If the red galaxies were more centrally concentrated than the blue, we could have incorporated it into our anal-

ysis by adjusting $\lambda(r|m)$. In fact, Fig. 2 of Diaferio et al. (1999) shows that, in the semianalytic model, the red galaxies in massive clusters are concentrated more towards the centres of their parent haloes than the blue ones are. The agreement between the simulation and our model curves in which we made no such adjustment for this suggests that it must amount to only a weak effect.

We turn, therefore, to the first and second moments of the pairwise velocity distribution for these four subsamples. Fig. 5 shows results for the same semianalytic galaxy samples shown in Fig. 4. As before, crosses, squares, triangles and open circles show galaxies classified as being red, quiescent, star-forming, or blue. Filled circles show the corresponding statistics of the dark matter particles. As for the correlation functions, the blue and star-forming samples are quite different from the red and quiescent samples. Our model shows that this arises simply from the fact that these samples have rather different $N_{\text{gal}}(m)$ relations—there are only a few blue, star forming galaxies in clusters.

Notice that blue galaxies (circles) have the smallest streaming motions, and red galaxies (crosses) have the largest v_{12} values. Our model predicts that larger streaming motions at large separations indicate a higher amplitude of clustering on those scales. Comparison with Fig. 4 shows that the correlation functions of the red galaxies are biased high relative to the dark matter, whereas the blue galaxies are biased low. This is in qualitative agreement with our model.

The solid lines in Fig. 5 provide a more quantitative comparison between our model predictions for the red and

blue galaxies, and the values of the galaxy velocities measured in the GIF simulation. The model predictions are in reasonable agreement with the simulation, although the agreement is certainly not as good as it was for the correlation functions. Sheth et al. (2000) discuss the reason for the overestimate in $v_{12}(r)$ on large scales (e.g., these models do not satisfy the integral constraint). The bottom panels show the ratio of the galaxy velocities to those of the dark matter; i.e., $b_{v_{12}} \equiv v_{12}^{\text{gal}}/v_{12}^{\text{dm}}$, and similarly for $b_{\sigma_{12}}$. This ratio is scale dependent on smaller scales. Our model describes the scale dependence reasonably well.

4 DISCUSSION

We presented a simple model of how the streaming motions of haloes and galaxies depends on separation. We tested the model using the publically available simulations of Kauffmann et al. (1999). In the semi-analytic galaxy formation model, the mean streaming motions depend rather strongly on how the galaxy sample was selected. For example, blue galaxies have smaller streaming motions than red galaxies. We showed that our model was able to describe the differences between a wide range of simulated galaxy catalogues rather well (Fig. 5).

Our model predicts a very close relationship between the streaming motions of the galaxies and their spatial distribution. Optical and IRAS galaxies cluster differently (e.g. Marzke et al. 1995; Fisher et al. 1994). Therefore, they must be biased differently relative to the dark matter. If the streaming motions of optical galaxies are the same as the dark matter, then our model predicts that the streaming motions of IRAS galaxies must be different from that of the dark matter. In other words, whether or not the streaming motions of a given galaxy sample trace the motions of the underlying dark matter depends on how the sample was selected. Thus, in the absence of strong arguments for why a given galaxy sample is expected to be unbiased, one should be cautious when interpreting measurements of the streaming motions of galaxies.

If the correlation function and the streaming motions of two different galaxy samples have been measured, then the model described here (equations 11 and 14) says that the square root of the ratio of the two correlation functions (at, say, 20 Mpc/h) should equal the ratio of the streaming motions on the same scale. This can be used to test the validity of the model. Again, however, caution is required because this relationship is only true on large scales. For the semi-analytic galaxy samples we presented, this simple linear biasing was a good approximation on scales larger than about 10 Mpc/h (although our model is able to describe the scale dependence of this ratio even on smaller scales). In this context, we think it worth noting that the semi-analytic galaxy samples we presented here cannot explain the results of Juszkiewicz et al. (2000) who found that ellipticals and spirals have the same value of v_{12} on separations of about 10 Mpc/h, even though they estimate that the spatial distributions have bias factors which differ by a factor of two: $b_E/b_S \approx 2$. It will be interesting if future data sets confirm this.

In addition to studying how the mean streaming velocity depends on galaxy type, our Fig. 5 also shows that the

second moment of the pairwise velocity distribution depends strongly on galaxy type. For example, our model of the pairwise dispersion suggests that the dispersion of blue galaxies should be substantially smaller than that of red ones (although this difference depends on the colour cut), especially on scales of 1 Mpc/h or so. Thus, it is not surprising that σ_{12} for optical galaxies (Marzke et al. 1995) is almost a factor of two larger than for IRAS galaxies (Fisher et al. 1994). The effects of redshift space distortions are larger if the pairwise dispersion is larger. This means that, on small scales, the amplitude of the redshift space correlation function of red galaxies should be substantially smaller than the real space correlation function, but the difference between real and redshift space correlation functions of blue galaxies should not be as dramatic. This is a generic prediction of these sorts of galaxy formation models. This suggests that galaxy redshift samples cut by colour should provide a useful and direct test of these models.

Dividing a galaxy sample by colour allows another simple test of these models. At large separations, where most pairs are in separate haloes, the model described above predicts that the cross-correlation function of the two colour samples should simply be the geometric mean of the two individual samples. If the two galaxy samples both trace their parent dark matter haloes in the same way (our Fig. 4 shows that this assumption describes the semianalytic model well), then this will be approximately true even on smaller scales. (It will not be exactly true because the scatter in the $N_{\text{gal}}(m)$ relations are, typically, sub-Poisson.) Data sets currently available should be able to test this prediction.

ACKNOWLEDGMENTS

This collaboration was started at the German American Young Scholars Institute in Astroparticle Physics, at the Aspen Center for Physics in the fall of 1998, and at Ringberg Castle in 1999. RKS thanks the IAS, as well as the University and Observatory at Torino, and LH & RS thank Fermilab for hospitality where parts of this work were done. We all thank the Halo Pub for inspiring nourishments. The N-body simulations, halo and galaxy catalogues used in this paper are publically available at <http://www.mpa-garching.mpg.de/NumCos>. The simulations were carried out at the Computer Center of the Max-Planck Society in Garching and at the EPCC in Edinburgh, as part of the Virgo Consortium project. In addition, we would like to thank the Max-Planck Institut für Astrophysik where some of the computing for this work was done. RKS is supported by the DOE and NASA grant NAG 5-7092 at Fermilab. LH is supported by NASA grant NAG5-7047, NSF grant PHY-9513835 and the Taplin Fellowship. He also thanks the DOE for an Outstanding Junior Investigator Award (grant DE-FG02-92-ER40699) RS is supported by endowment funds from the IAS and by NSF grant PHY-0070928 at IAS.

REFERENCES

- Diaferio A., Kauffmann G., Colberg J., White S. D. M., 1999, MNRAS, 307, 537
 Fisher et al. 1994, MNRAS, 267, 927

- Hamilton A. J. S., Kumar P., Lu E., Matthews A., 1991, ApJ, 374, L1
- Kauffmann G., Colberg J., Diaferio A., White S. D. M., 1999, MNRAS, 303, 188
- Juszkiewicz R., Ferreira P. G., Feldman H. A., Jaffe A. H., Davis M., 2000, Science, 287, 109
- Ma C. P., Fry J., 2000, ApJ, submitted
- Marzke et al. 1995, AJ, 110, 477
- Mo H. J., White S. D. M., 1996, MNRAS, 282, 347
- Mo H. J., Jing Y. P., Börner G., 1997, MNRAS, 286, 979
- Nityananda R., Padmanabhan T., 1994, MNRAS, 271, 976
- Peacock J., Smith R., 2000, MNRAS, submitted, astro-ph/0005010
- Peebles P. J. E., 1980, The Large Scale Structure of the Universe. Princeton Univ. Press, Princeton
- Press W., Schechter P., 1974, ApJ, 187, 425
- Seljak U., 2000, MNRAS, in press, astro-ph/0001493
- Scoccimarro R., Sheth R. K., Hui L., Jain B., 2000, ApJ, accepted, astro-ph/0006319
- Sheth R. K., Saslaw W. C., 1994, ApJ, 437, 35
- Sheth R. K., Diaferio A., 2000, MNRAS, submitted, astro-ph/0009166
- Sheth R. K., Hui L., Diaferio A., Scoccimarro R., 2000, MNRAS, submitted, astro-ph/0009167

APPENDIX A: THE EVOLUTION OF THE CORRELATION FUNCTION

This Appendix shows how the correlation function and the mean streaming motions evolve in our model.

The correlation function on comoving scale x when the expansion factor is a is the sum of two terms:

$$\xi_{\text{dm}}(x, a) = \xi_{\text{dm}}^{\text{1halo}}(x, a) + \xi_{\text{dm}}^{\text{2halo}}(x, a), \quad (\text{A1})$$

where

$$\xi_{\text{dm}}^{\text{2halo}}(x, a) = \xi_{\text{dm}}^{\text{Lin}}(x, a) \left[\int dm f(m) b(m, a) \right]^2 \quad (\text{A2})$$

(compare equation 13), and

$$\xi_{\text{dm}}^{\text{1halo}}(x) = \int dm \frac{m^2 n(m)}{\bar{\rho}} \frac{\lambda(x|m)}{\bar{\rho}}. \quad (\text{A3})$$

For haloes of virial mass m which have density profiles of the form given by Navarro, Frenk & White (1997),

$$\lambda(x|m) = \frac{c^3 \phi^2(c)}{4\pi r_{\text{vir}}^3} g\left(\frac{cx}{x_{\text{vir}}}\right), \quad (\text{A4})$$

where $g(y)$ is given in Appendix A3 of Sheth et al. (2000). Here r_{vir} is the virial radius of the halo in proper physical coordinates, $x_{\text{vir}} = r_{\text{vir}}/a$ is the comoving virial radius, and $c(m)$ is a parameter which describes how centrally concentrated the halo profile is: it is the ratio of the virial radius to a central core radius, and it depends on the halo mass. The normalization term is

$$\phi(c) \equiv \left[\ln(1+c) - c/(1+c) \right]^{-1}. \quad (\text{A5})$$

The mean streaming motions from pairs in the same halo is given by equation (10) in the main text.

We would like to study what happens if we make the profile of the region containing m depend on time in the following way: we would like to use the same family of profiles, such as the NFW set, to describe the density run at

any time, and we want to parametrize the evolution of the profile shape by changing the values of the profile's parameters. There is no physical reason why the NFW form should describe the density run around a region which has yet to virialize; we are only using this to illustrate how our argument works.

For NFW profiles, this means that we will think of $X(a) = X_a$ as the comoving boundary of the region containing m at the time when the expansion factor is a : initially $X(a_i) = X_i$, and today $X(a_0) = x_{\text{vir}}$. In addition, we will allow the concentration parameter to depend on mass as well as time: $c(m, a) = c_a$. The idea is that the density run around the centre of the region of radius X_a containing m was presumably differently concentrated at a_i than it is today. In particular, we would like to see if this model can produce the same streaming motions as equation (10) in the main text.

To show what is required for this to happen, set $mn(m)/\bar{\rho} = f(m)$, and also set $m = 4\pi X_i^3 \bar{\rho}_0/3$, where X_i is the initial comoving radius of the halo, and $\bar{\rho}_0 = \bar{\rho}/a^3$ is the comoving density of the background. Then the expression for the correlation function becomes

$$\xi_{\text{dm}}^{\text{1halo}}(x) = \int dm f(m) \left(\frac{c_a X_i}{X_a} \right)^3 \frac{\phi^2(c_a)}{3} g\left(\frac{c_a x}{X_a}\right). \quad (\text{A6})$$

The volume integral of this is

$$\begin{aligned} \bar{\xi}(x) &= \int dm f(m) \left(\frac{c_a X_i}{X_a} \right)^3 \frac{\phi^2(c_a)}{x^3} \int_0^x dy y^2 g\left(\frac{c_a y}{X_a}\right) \\ &= \int dm f(m) \phi^2(c_a) \left(\frac{X_i}{x} \right)^3 \bar{g}\left(\frac{c_a x}{X_a}\right), \end{aligned} \quad (\text{A7})$$

where we have defined $\bar{g}(y) \equiv \int_0^y dz z^2 g(z)$. So

$$\begin{aligned} \frac{\partial \bar{\xi}(x)}{\partial \ln a} &= \int dm f(m) \left[\frac{\partial \ln \phi^2(c_a)}{\partial \ln a} \left(\frac{X_i}{x} \right)^3 \phi^2(c_a) \bar{g}\left(\frac{c_a x}{X_a}\right) \right. \\ &\quad \left. + \frac{\partial \ln(c_a/X_a)^3}{\partial \ln a} \frac{\phi^2(c_a)}{3} \left(\frac{c_a X_i}{X_a} \right)^3 g\left(\frac{c_a x}{X_a}\right) \right]. \end{aligned} \quad (\text{A8})$$

This will result in the same streaming motions as equation (10) if

$$\begin{aligned} \frac{\partial \ln \phi^2(c_a)}{\partial \ln a} &= \frac{6f_{\Omega}}{3+n_*} \quad \text{and} \\ \frac{\partial \ln(c_a/X_a)^3}{\partial \ln a} &= -\frac{6f_{\Omega}}{3+n_*}, \end{aligned} \quad (\text{A9})$$

where n_* is the slope of the linear power spectrum on the scale on which the rms density fluctuation is 1.686, and $f_{\Omega} \equiv \partial \ln D(a)/\partial \ln a \approx \Omega^{0.6}$, where $D(a)$ is the linear theory growth factor. This sums up what is required of the time dependence of the concentration c_a and the comoving radius X_a containing m . Note that these requirements are non-trivial, because both c and X depend on the mass m , but we are requiring that the derivatives work out to be independent of m .

We can see what this implies for the evolution of the correlation function if we insert the scalings of equation (A9) in equation (A6):

$$\xi_{\text{dm}}^{\text{1halo}}(x, a) = \int dm f(m) \left(\frac{c_0 X_i}{X_0} \right)^3 \frac{\phi^2(c_0)}{3} g\left(\frac{c_0 x/X_0}{D^{2/(3+n)}}\right),$$

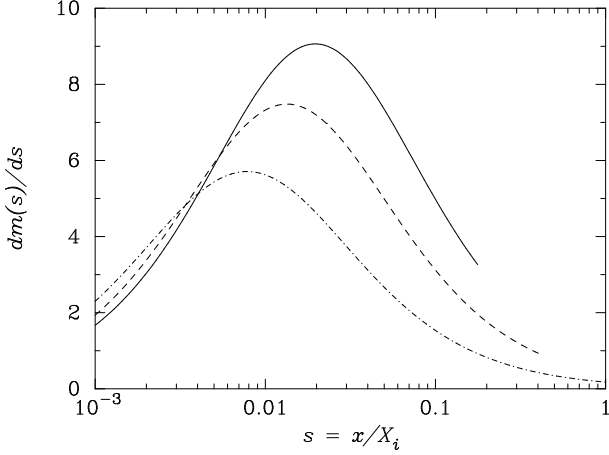


Figure A1. The evolution of the mass profile if we require that the density profile have the NFW form at all times. For most of the comoving volume, the mass in a given comoving shell increases with time. Only within the core of the object does the mass decrease with time. We have truncated the profiles at the point where they all enclose the same mass m .

where the subscript ‘0’ denotes the values of quantities at the present time. This shows that the number of pairs on comoving scale x at the present time is the same as the number of pairs which, at the earlier time when the linear growth factor was $D = D(a)/D_0$ were on the larger comoving scale $x/D^{2/(3+n)}$.

The correlation function decreases monotonically with scale, so the expression above implies that $\xi_{\text{dm}}^{\text{halo}}$ was smaller at early times than it is today. At very early times, therefore, the correlation function might plausibly be dominated by the two-halo term (equation A2). The evolution of this term can be got from inserting the evolution of the bias factor (equation 4) into it. The integrals over m can be done analytically, with the result that $\xi_{\text{dm}}^{\text{halo}}(x, a) = D^2 \xi_{\text{dm}}^{\text{Lin}}(x, a_0)$. At sufficiently early times, this two-halo term dominates on all scales, so our model for the correlation function reduces correctly to the linear theory expression.

Our requirement that the same NFW form hold at all times means that the profile shape evolves as

$$\begin{aligned} \frac{\rho_a(s)}{\bar{\rho}} &= \frac{\phi(c_a)/3}{s(s + (X_a/c_a)/X_i)^2} \\ &= \frac{\rho_{a_0}(S)}{\bar{\rho}_0} D^{3/(3+n_*)} \left(\frac{S + 1/c_0}{S + D^{2/(3+n)}/c_0} \right)^2, \end{aligned} \quad (\text{A10})$$

where s is the comoving distance from the centre in units of the initial comoving scale X_i , whereas S is in units of the virial radius at a_0 . The second equality follows from the scalings above for the evolution of $\phi(c_a)$ and X_a/c_a , and setting $D \equiv D(a)/D_0$. The profile evolves in such a way that the density on scales $s > (X_a/c_a)/X_i$ grows as a increases, as we expect. On much smaller scales, $s \ll (X_a/c_a)/X_i$, and the profile shape is more like $(c_a X_i/X_a)^2 \phi(c_a)/S \propto D^{-1/(3+n)}/S$: on very small scales, the density decreases with time!

Because this small scale behaviour of the density seems contrary to our intuition, we thought it worth studying the evolution of the mass as a function of comoving scale. The scalings above imply that the fraction of the total mass $m =$

$M(s)/M$ which is in the range ds around s from the halo centre when the growth factor is $D \equiv D(a)/D_0$ is

$$\frac{dm(s)}{ds} \propto \frac{s\phi(c_0)D^{3/(3+n_*)}}{\left[s + D^{2/(3+n_*)}/[c_0(\Delta_{\text{nl}}/\Omega)^{1/3}] \right]^2}. \quad (\text{A11})$$

Fig. A1 shows an example of how the mass gets redistributed as the profile evolves. It was constructed by setting $n_* = -1.5$, $c_0 = 9$ and $D_{\text{nl}}/\Omega = 180$ in equation (A11) (the first two values approximate those of an m_* halo in a Λ CDM simulation). The solid, dashed, and dot-dashed curves show equation (A11) at $D = 1, 0.75$ and 0.5 respectively. For most of the volume of the halo, the mass in a given comoving shell increases as D increases. Only well within the core of the object does it decrease with time. We only show the shape of the profile out to the radius X_a which contains the mass m . At $D = 1$, X_a is the virial radius, which is at $s = 1/5.6 \approx 0.18$; X_a was larger earlier, so that the total mass contained in the profile remains constant. By $D = 0.6$ or so $X_a > 1$, indicating that the model profile must extend beyond X_i if it is to enclose mass m ; at this point the model has really broken down.

A similar analysis of the Hernquist profile shows the same qualitative features:

$$\frac{\rho_a(S)}{\bar{\rho}} = \frac{\rho_{a_0}(S)}{\bar{\rho}_0} D^{5/(3+n_*)} \left(\frac{S + b_0}{S + b_0 D^{2/(3+n_*)}} \right)^3. \quad (\text{A12})$$

Presumably, this apparently unphysical behaviour is a consequence of our unphysical requirement that the profile have the same functional form at all times.